Journal of Statistical Physics, Vol. 57, Nos. 3/4, 1989

New Methods for Calculating the Dew/Bubble Curves of Classical Model Fluids

J. M. Kincaid,[1] K. B. Shon,[1] and G. Fescos[1]

Received March 3, 1989

We describe two new methods for locating the dew/bubble curves of fluids. One is a numerical method and the other an analytical method based on the use of series expansions. The utility of these two methods is illustrated by application to a simple one-component fluid model and to several model polydisperse fluids. The numerical method is based on a new geometric representation of the equilibrium conditions—similar in spirit to the geometric representations often used for solving the equilibrium conditions of pure fluids. Our calculations show that the series-expansion technique can be quite effective at producing accurate representations of the phase boundaries.

KEY WORDS: Coexistence curve; critical point; dew/bubble curve; phase transitions; polydisperse; series expansions.

1. INTRODUCTION

In this paper we shall describe a new approach to locating the phase boundaries of fluids. Although there is a vast literature on the formal physical theory of phase transitions, only a handful of techniques have been developed for putting the formal theory to good use. The "good use" we speak of here can be divided into two categories: (1) the explication of model systems whose properties are intended to provide a fundamental description of some real system; and (2) engineering calculations necessary to the design of processes in which phase transitions occur. An example from the first category is provided by the work of van Leeuwen and Cohen[1] on the hard-sphere Fermi–Bose model of ^{3}He–He^4 mixtures. Starting with the assumption that quantum statistics and excluded-volume

[1] Department of Mechanical Engineering, SUNY at Stony Brook, Stony Brook, New York 11794.

0022-4715/89/1100-0937$06.00/0

effects play a dominant role in determining the properties of liquid helium, van Leeuwen and Cohen began a very fruitful investigation into the properties of a mixture of hard-sphere fermions and bosons. Using both numerical and analytical techniques, they found that their model for ^{3}He–He^4 mixtures exhibited a quite interesting variety of phase behavior that subsequent experiments confirmed. An example drawn from the second category is provided by the problem of heat engine design.[2] In order to simulate the operation of a heat pump under a variety of operating conditions, it is necessary to determine the state of the working fluid in all regions of the apparatus. This requires accurate representations of the phase boundaries, and in the case of designs that use mixtures as the working fluid, may require that phase equilibrium calculations be calculated, so to speak, "on the fly." In each case, the two-phase equilibrium conditions must be solved for a range of thermodynamic states.

The "good use" is therefore limited by our ability to obtain *solutions* to the equilibrium conditions. This paper describes two new methods for finding these solutions. Our original motivation for developing these methods was to make possible accurate phase equilibrium calculations on systems containing a large number of species, such as petroleum fluids. We find, however, that they can be quite useful even for pure fluids. The first method is a numerical procedure based upon a simple reformulation of the equilibrium conditions; it is founded on a simple geometric representation of the (reformulated) equilibrium conditions. The second is an analytical approach that relies on the application of series-expansion techniques. These two methods provide solutions to the equilibrium conditions of one-component fluids, multicomponent fluids, and polydisperse fluids. In both cases we limit our discussion to a special subset of the equilibrium conditions: the dew/bubble conditions. These conditions involve a smaller set of dependent variables than the full equilibrium conditions and are therefore easier to solve.

For the remainder of this section we review some of the solution methods that are commonly used. In Sections 2 and 3 we illustrate our new methods on one-component and multicomponent systems, respectively. Section 4 contains our concluding remarks and suggestions for future work.

1.1. One-Component Fluids ($C=1$)

In the case of fluids containing only a single species of particles the phase boundary, or coexistence curve, is identical to the dew/bubble curve. The (local) equilibrium conditions are[3]

$$p(T, x) = p(T, y) \tag{1}$$

and

$$\mu(T, x) = \mu(T, y) \tag{2}$$

where T is the temperature, x and y are the number densities of two coexisting phases, p is the pressure, and μ is the chemical potential. The problem is: given T (less than the critical temperature T_c), find x and y. [If the total system density ρ is fixed, then an additional equation, $\rho = \phi/x + (1-\phi)/y$, must be added, where ϕ is the number fraction of particles in the phase with density x. Since this conservation equation may be easily solved for ϕ in terms of x, y, and ρ, this problem is really no harder than solving Eqs. (1) and (2).] There are three standard techniques for solving these equations: the equal-areas method, the bitangent construction, and the minimization of $\mu(T, p)$. Each method has a simple geometric interpretation and the numerical implementation of each method relies heavily on the geometric interpretation. These three methods are so well-known that we will not describe them in any detail except to point out that each one restates the equilibrium conditions in a manner that leads to a straightforward geometric representation. In Fig. 1 we draw p and μ as functions of the density for the van der Waals model at a temperature below the critical temperature. It is not obvious from these graphs which

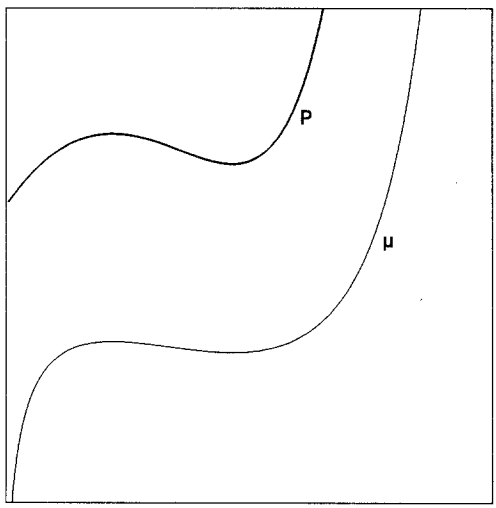

Fig. 1. The pressure p and chemical potential μ (Gibbs free energy per particle) as a function of density for the van der Waals model at constant temperature ($T = 0.8T_c$). It is not obvious from these curves which densities satisfy the equilibrium conditions.

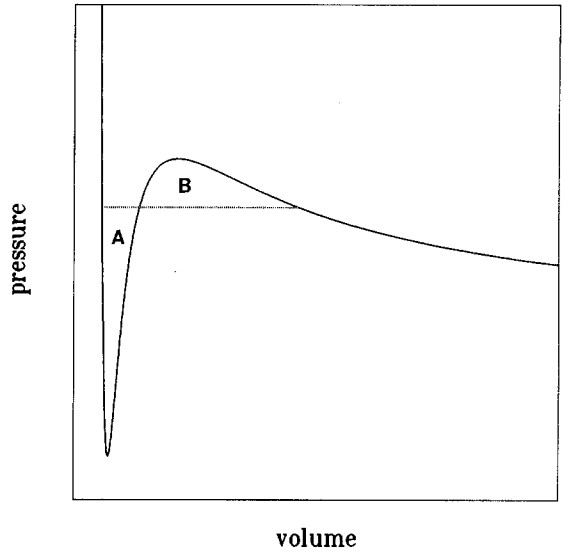

Fig. 2. The pressure as a function of volume (per particle) for the same conditions as Fig. 1. The equal-areas rule states that the equilibrium conditions are satisfied when volumes v_1 and v_2 are chosen such that areas A and B are equal. It is not difficult to obtain a good approximation to v_1 and v_2 by inspection.

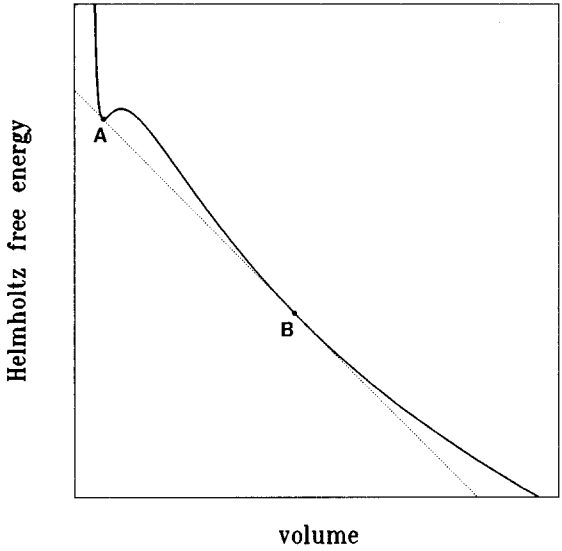

Fig. 3. The Helmholtz free energy as a function of volume (per particle) for the same conditions as Fig. 1. The bitangent construction solves the equilibrium conditions by locating points A and B such that the line AB has slope $-p$ and is tangent to the curve at A and B.

densities x and y will satisfy Eqs. (1) and (2). Although a numerical solution of these equations is not too difficult to obtain by patient trial and error, the geometric representations (see Figs. 2–4) immediately suggest reasonable guesses for an approximate solution *and* simple numerical algorithms for finding the exact solution. Moreover, the shapes of the curves in Figs. 2–4 provide useful information about the numerical precision that will be required. The locus of densities x and y that satisfy Eqs. (1) and (2) for $T \leqslant T_c$ comprise the coexistence curve, shown in Fig. 5.

1.2. Multicomponents Fluids ($C > 1$)

In the case of mixtures the equilibrium conditions are more difficult to solve because there are additional thermodynamic variables. In a C-component mixture the state of any phase is determined by T, ρ, and $C-1$ mole fractions. For an isothermal system at temperature T, density ρ, with mole fractions $\{f_i\}$, the equilibrium conditions are[3]

$$p(T, x, \{f_{xj}\}) = p(T, y, \{f_{yj}\}) \tag{3}$$

$$\mu_i(T, x, \{f_{xj}\}) = \mu_i(T, y, \{f_{yj}\}), \qquad i = 1,..., C \tag{4}$$

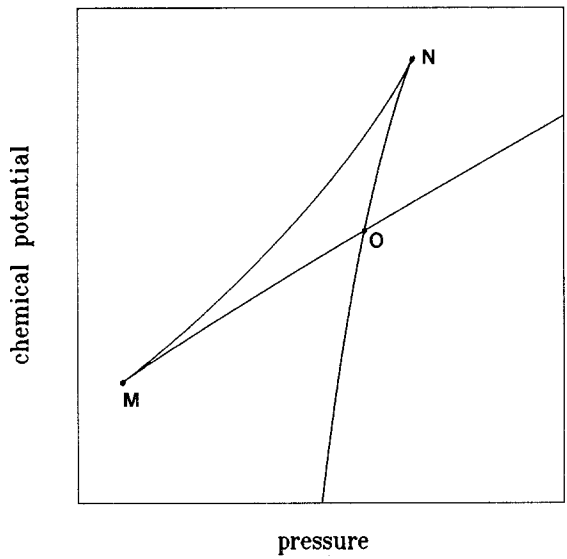

Fig. 4. The chemical potential (Gibbs free energy per particle) as a function of pressure for the same conditions as Fig. 1. The equilibrium states are those which minimize the chemical potential for a given p. Thus, the "hat" MNO does not represent equilibrium states (except at the point O). Two-phase equilibrium occurs at the point O; the volumes per particle of the coexisting phase are given by the two values of $(\partial\mu/\partial p)_T$ at that point.

$$\frac{1}{\rho} = \phi \frac{1}{x} + (1-\phi)\frac{1}{y} \tag{5}$$

$$f_i = \phi f_{xi} + (1-\phi) f_{yi} \tag{6}$$

and

$$\sum_{i=1}^{C} f_{xi} = \sum_{i=1}^{C} f_{yi} = 1 \tag{7}$$

Here x and y are the number densities of the two coexisting phases with mole fractions $\{f_{xj}\}$ and $\{f_{yj}\}$, respectively.

When C is greater than 2, these equations can be quite difficult to solve for x, y, ϕ, $\{f_{xj}\}$, and $\{f_{yj}\}$. The principal source of difficulty is due to the lack of a clear geometric representation of the equilibrium conditions. A somewhat simpler problem is to locate the boundary of the two-phase region. This is the dew/bubble problem and we shall focus attention on it. The dew/bubble conditions are obtained by seeking only those

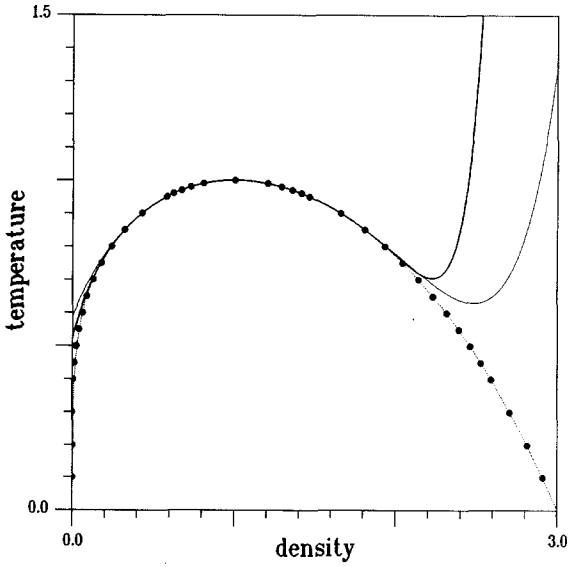

Fig. 5. The coexistence curve of the van der Waals model in the temperature–density plane. (The units are chosen such that $T_c = X_c = 1$.) The dots represent coexisting states determined using the equal-areas rule; the series-expansion results are represented by the solid curves: the thick curve comes from the 15-term series, the thin curve comes from the 7-term series. The dotted curve represents the [7/8] Padé of the 15-term series. The Padé was constructed to ensure that the correct $T = 0$ result was obtained.

solutions of Eqs. (3)–(7) for which $\phi \to 1$ (or $\phi \to 0$). In this case, given T and $\{f_j\}$, one must determine x, y, and $\{f_{yj}\}$ such that

$$p(T, x, \{f_j\}) = p(T, y, \{f_{yj}\}) \tag{8}$$

$$\mu_i(T, x, \{f_j\}) = \mu_i(T, y, \{f_{yj}\}), \qquad i = 1,..., C \tag{9}$$

and

$$\sum_{i=1}^{C} f_{yi} = 1 \tag{10}$$

Here x is the density of the phase for which $\phi \to 1$; thus, it is the "bulk phase"; y is the density of the second phase, that is "just barely present" since $(1-\phi) \to 0$; the y phase is called the dew or bubble, depending on whether y is greater than or less than x. The locus of points (x, T) is called the dew/bubble curve and the locus of points (y, T) is called the shadow curve; we shall refer to these curves collectively as the dew/bubble curves. A set of typical curves is shown in Fig. 6. The pairs of points A_1, A_2 and

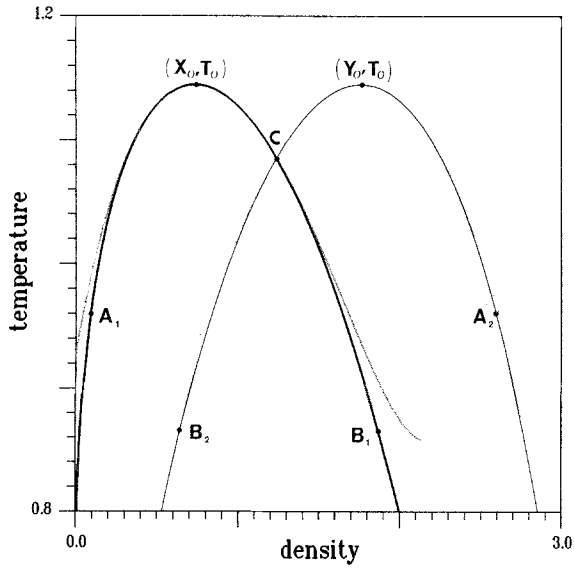

Fig. 6. The dew/bubble (thick curve) and shadow (thin curve) curves for model 2 in the temperature–density plane for $v = 5$. Two sets of coexisting phases are represented by the points (A_1, A_2) and (B_1, B_2). The points A_1 and B_1 lie on the dew/bubble curve, representing the total system density at which a second phase just begins to appear. The points A_2 and B_2 lie on the shadow curve, representing the density of the second phase. The dotted curves represent the 5-term series-expansion result. (X_0, T_0) and (Y_0, T_0) are the condenterm points; C is the critical point (X_c, T_c).

B_1, B_2 represent pairs of coexisting phases; the point C is the critical point (X_c, T_c); the points (X_0, T_0) and (Y_0, T_0) are called the condentherm points. In a one-component system the dew/bubble and shadow curves are identical, as are the points (X_c, T_c), (X_0, T_0), and (Y_0, T_0). The dew/bubble and shadow curves are projections of a slice of the full coexistence surface onto the T–ρ plane, and as such they convey only limited information about the coexistence surface. In particular, they do not indicate the composition of the y phase, nor do they describe the state of the system when the total density lies within the dew/bubble curve—except that in this region the system is known to be in a two-phase state.

While the dew/bubble conditions involve fewer variables, and are therefore easier to solve than the full equilibrium conditions, they are still quite difficult to solve. Although there are higher-dimensional analogs of the bitangent and minimization-of-μ methods used for one-component systems, they have not yet proved to be of much general use. We believe that this stems from the lack of a clear geometric picture of the functions involved. When $C > 3$ one usually resorts to numerical methods for solving nonlinear simultaneous equations that make only limited use of thermodynamics. We shall refer to those methods as "blind-search" methods. (These methods, the best of which can be quite sophisticated, are "blind" is the sense that very little, if any, knowledge of thermodynamics is built into their algorithms.)

1.3. Polydisperse Systems ($C \to \infty$)

When the number of components becomes extremely large, as is the case in many polymer and petroleum applications, it has proved convenient to model those systems as though $C = \infty$, replacing the discrete species index i by a continuous species label I. In these cases the mole fractions $\{f_i\}$ are represented by a mole-fraction density function $F(I)$. Locating the phase boundaries of a polydisperse system is in some sense the ultimate phase equilibrium problem. It is hard to imagine a more difficult problem within this class. The dew/bubble conditions become three coupled nonlinear integral equations and the phase space becomes infinite-dimensional.

The extreme computational difficulty posed by the polydisperse problem does have a major advantage: it makes "blind-search" methods appear quite infeasible. The study of phase equilibrium in polydisperse systems has therefore focused on the development of new solution methods.[4–16] In particular, we have, along a somewhat parapetetic path, been led back to search for essentially geometric formulations of the equilibrium conditions that have sensible projections onto a two-dimensional

space. While we cannot claim to have completely succeeded in doing this, we believe that the work described in the following sections is *on the right track*. We have found a simple reformulation of the dew/bubble conditions that leads to a simple two-dimensional representation of the dew/bubble conditions for a broad class of model fluids. The method works for one-component, multicomponent, and polydisperse fluids. In addition to suggesting numerical solution algorithms, it has led to a straightforward analytical solution method by series expansion. The latter method is only "new" in the sense that apparently no one thought it would yield usefully accurate solutions. The series-expansion method has been used for many years to elucidate the properties of phase boundaries near the critical point.[17–19] We have simply gone one step further: having understood the geometry of the dew/bubble curves, we merely extended the method to the entire coexistence surface.

2. ONE-COMPONENT MODELS

The problem here is: for a specified temperature T ($<T_c$), find densities x and y such that Eqs. (1) and (2) are satisfied. By making some rather trivial modifications of the these equations, we have come upon an alternative geometric representation that has proved to be quite useful. We begin by introducing two functions $f(T, x, y)$ and $g(T, x, y)$ defined by

$$f(T, x, y) = p(T, x) - p(T, y) \tag{11}$$

and

$$g(T, x, y) = \exp\left[\frac{\mu(T, x) - \mu(T, y)}{k_B T}\right] - 1 \tag{12}$$

Clearly, if

$$f(T, x, y) = 0 \tag{13}$$

and

$$g(T, x, y) = 0 \tag{14}$$

then Eqs. (1) and (2) are satisfied. Although this form of the equilibrium conditions is hardly different from Eqs. (1) and (2), the definitions of f and g immediately suggest that the trivial solution $x = y$ can be factored out. Thus, we define two new functions $\tilde{f}$ and $\tilde{g}$ by

$$\tilde{f}(T, x, y) = f(T, x, y)/(x - y) \tag{15}$$

$$\tilde{g}(T, x, y) = g(T, x, y)/(x - y) \tag{16}$$

The equilibrium conditions may now be expressed as

$$\tilde{f}(T, x, y) = 0 \tag{17}$$

$$\tilde{g}(T, x, y) = 0 \tag{18}$$

This form of the equilibrium conditions is especially useful for models in which the pressure is a rational function of the density. In these cases the trivial solution can be factored out by explicitly, and the polynomial represented by $\tilde{f} = 0$ is one degree lower than that represented by $f = 0$. In particular, if the equation of state is "cubic" (as in the van der Waals model), then the roots of the first equilibrium condition can be obtained by solving a quadratic equation! Generally $\tilde{g}$ involves transcendental functions, so the term $(x - y)$ cannot be divided out explicitly. [It is also possible to define g as the difference of the chemical potentials, but μ always contains logarithmic terms and Eq. (12) has the advantage of eliminating those terms.]

2.1. The Geometry of the Curves $\tilde{f} = 0$ and $\tilde{g} = 0$

Equations (17) and (18), for a given T, define two curves in the x–y plane. We shall refer to these curves as the f and g curves, respectively. The solution of the equilibrium conditions is represented by the points of intersection of the f and g curves. When $p(T, \rho)$ has a single "van der Waals wiggle" the f and g curves will be represented by single, closed loops in the x–y plane. These curves will be symmetric about the line $x = y$. For $T > T_c$, the f and g curves do not exist [i.e., there are no real roots to Eqs. (17) and (18)]. For $T < T_c$ the f and g curves intersect at four points. Two of these four points are the spinodal points defined by $(\partial p/\partial \rho)_T = 0$. At these points the f and g curves cross the line of trivial solution $x = y$ with a slope of -1. That is, the f and g curves are tangent when they cross the line $x = y$ and they are perpendicular to that line. The remaining two points of intersection are symmetric about the line $x = y$ and represent the desired solutions of the equilibrium conditions. As $T \to T_c$ from below, the f and g curves shrink to a point at $x = y = \rho_c$. In Figs. 7 and 8 we draw the f and g curves for several temperatures for the van der Waals model and for a hard-sphere based model of refrigerant R-12.[20] Although the equations of state of these two models differ in their dependence on T and ρ, the f and g curves are qualitatively similar.

2.2. Numerical Solutions

A new technique for numerically solving the equilibrium conditions is suggested by the geometry of Eqs. (17) and (18): simply to follow the f

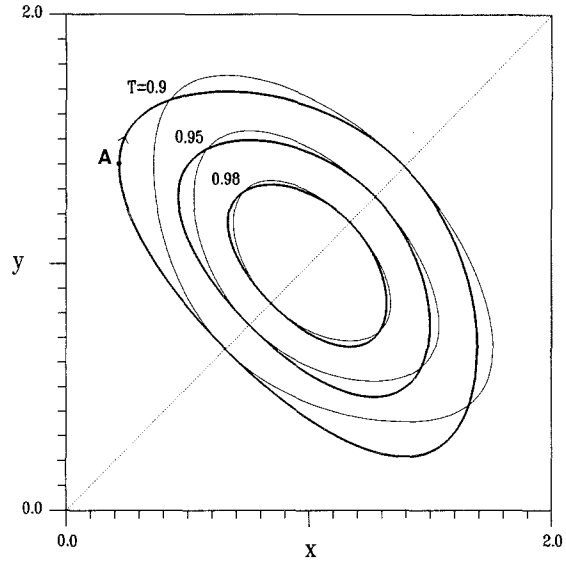

Fig. 7. The f and g curves (thick and thin curves, respectively) for the one-component van der Waals model in the density–density plane for $T=0.9$, 0.95, and 0.98. The curves are symmetric about the line of trivial solutions $x=y$. The locus of nontrivial intersections of the f and g curves gives the density of coexisting phases. As the temperature approaches the critical temperature $T=1$, both curves shrink to a point at $x=y=1$, the critical density. The f–g intersection is located numerically by starting at the point A and following the f curve until it crosses the g curve.

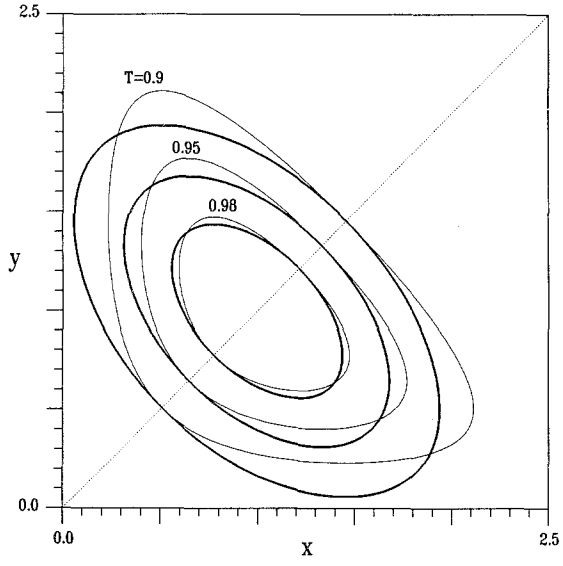

Fig. 8. The f and g curves (thick and thin curves, respectively) for R-12 in the density–density plane for $T=0.9$, 0.95, and 0.98. These curves are qualitatively the same as those of the van der Waals model. The small difference in shape is due to the stronger interparticle repulsion built into the R-12 model.[20]

curve until it intersects the g curve, as schematically shown in Fig. 7. More specifically: choose an x, find y by solving $\tilde{f}(T, x, y) = 0$, substitute x and y into $\tilde{g}$. If $\tilde{g} = 0$, then you have solved the equations. In the case of cubic equations of state, one obtains two solutions to Eq. (17) for a given x, call them $y_1(x)$ and $y_2(x)$. Because the $\tilde{f}$ and $\tilde{g}$ curves are symmetric about the line $y = x$, only one of the solutions is needed. Choosing $y_1(x)$, solving Eq. (18) is reduced to locating the zeros of the function $\tilde{g}(x, y_1(x))$. Since $\tilde{g}$ is >0 outside the $\tilde{g}$ curve and <0 inside the $\tilde{g}$ curve, locating the zero of $\tilde{g}$ is straightforward.

In the case of the van der Waals model, this method is especially simple. Using units such that $T_c = \rho_c = 1$, the van der Waals model, this method is especially simple. Using units such that $T_c = \rho_c = 1$, the van der Waals pressure is given by

$$p(T, \rho) = \frac{8T\rho}{3 - \rho} - 3\rho^2 \tag{19}$$

$\tilde{f} = 0$ implies

$$0 = (8T - 9x + 3x^2) + (6x - x^2 - 9)\, y + (3 - x)\, y^2 \tag{20}$$

which has two real roots if and only if $T < 1$:

$$y(T, x) = \frac{3 - x}{2} \pm \left[\frac{27 - 32T + 9x - 3x^2 - x^3}{4(3 - x)} \right]^{1/2} \tag{21}$$

$\tilde{g}(T, x, y)$ is given by

$$\tilde{g}(T, x, y) = \left\{ \frac{x(3 - y)}{y(3 - x)} \exp\left[\frac{x}{3 - x} - \frac{y}{3 - y} - \frac{9(x - y)}{4T} \right] - 1 \right\} (x - y)^{-1} \tag{22}$$

A graph of $\tilde{g}(T, x, y(T, x))$ versus x is given in Fig. 9 for the case $T = 0.9$. The quantity $\tilde{g}(T, x, y(T, x))$ is tangent to the line $\tilde{g} = 0$ at the spinodal points. The equilibrium conditions are solved numerically by starting at point A or B and following the curve until one locates that x for which $\tilde{g}(T, x, y(T, x)) = 0$.

2.3. Analytic Solutions

In recent years much has been written about the critical point properties of classical model fluids and how they differ from the critical point properties of real fluids.[18,19] In particular it is always noted that classical models are (usually) analytic functions of T and ρ in the vicinity of the

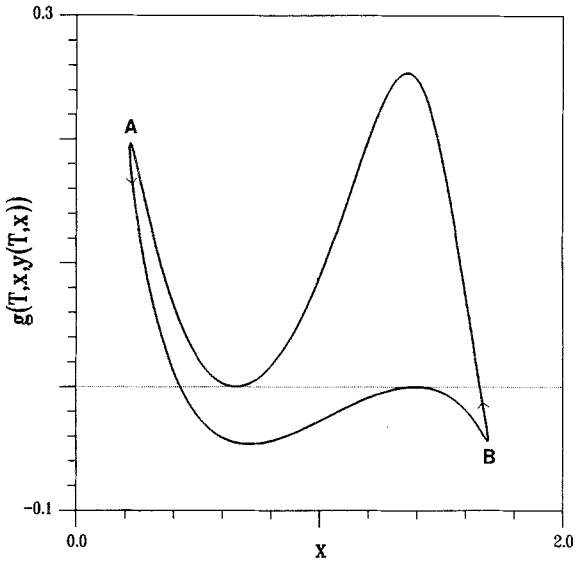

Fig. 9. Plot of $\tilde{g}$ as a function of density along the curve $\tilde{f}=0$ for the van der Waals model. ($T=0.9T_c$). The two branches of the curve result from the fact that for a given x there are two values of y such that $\tilde{f}=0$. The equilibrium conditions are solved by starting at either point A or point B and locating the points at which $\tilde{g}=0$.

critical point—guaranteeing critical behavior that is quite distinct from most real systems. But until recently this analytic behavior has not been exploited in phase equilibrium calculations. For one-component models, power series solutions of Eqs. (17) and (18) lead to quite accurate representations of the coexistence curve, as well as other thermodynamic properties on that curve.[9,21,22]

The functions $\tilde{f}$ and $\tilde{g}$ are particularly appropriate for such techniques. By choosing x to be the independent variable, we express the coexistence curve in terms of the expansions

$$T=T_c+\sum_{i=2}^{\infty} T_i(x-X_c)^i \tag{23}$$

and

$$y=X_c+\sum_{i=1}^{\infty} y_i(x-X_c)^i \tag{24}$$

The coefficients $\{T_i, y_i\}$ are determined by substituting these series into Eqs. (17) and (18), expanding $\tilde{f}$ and $\tilde{g}$ in powers of $(x-X_c)$, and setting the coefficients of each power of $(x-X_c)$ equal to zero. By using the

Gibbs–Duhem equation to relate density derivatives of μ to density derivatives of p, one can express the coefficients $\{T_i, y_i\}$ in terms of temperature and density derivatives of p alone. Kincaid *et al.*[22] have obtained T_2 through T_{13}, and y_1 through y_{12}. The first several coefficients are given in Table I. For any particular model a series representation of the coexistence curve may be obtained by "simply" evaluating derivatives of the pressure at the critical point. The details of those calculations, as well as application to several models, are presented in ref. 22. By forming Padé approximates of these series, very accurate approximations to the coexistence curve, as well as other thermodynamic functions on that curve, can be obtained.

In Fig. 5 we show the results for the van der Waals model.[9] The thick curve is the series representation of $T(x)$ using terms up to 15th order in $(x - X_c)$. The dotted curve is a [7/8] Padé approximant of the series. The

Table I. Coexistence Curve Series Coefficients for Pure (Classical) Fluids[a]

$$T_2 = -\frac{1}{6q_{11}} q_{30}$$

$$T_3 = -\frac{1}{90q_{11}^2} [3q_{11}q_{40} - (5q_{21} + 4q_{11})\, q_{30}] = -T_2 y_2$$

$$T_4 = -\frac{1}{5400q_{11}^3 q_{30}} [45q_{11}^2 q_{30}q_{50} - 18q_{11}^2 q_{40}^2 - 72q_{11}^2 q_{30}q_{40} - 150q_{11}q_{30}^2 q_{31} + 75q_{12}q_{30}^3 + (50q_{21}^2 + 200q_{11}q_{21} + 128q_{11}^2)\, q_{30}^2]$$

$$T_5 = -T_2 y_4 + 2T_2 y_2^3 - 2T_4 y_2$$

$$y_1 = -1$$

$$y_2 = -\frac{1}{15q_{11}q_{30}} [3q_{11}q_{40} - (5q_{21} + 4q_{11})\, q_{30}]$$

$$y_3 = -y_2^2$$

$$y_4 = -\{135q_{11}^3 q_{30}^2 q_{60} + [(315q_{11}^2 q_{21} + 144q_{11}^3)\, q_{30}^2 - 378q_{11}^3 q_{30}q_{40}]\, q_{50} - 630q_{11}^2 q_{30}^3 q_{41} + 378q_{11}^3 q_{40}^3 - (1134q_{11}^2 q_{21} + 756q_{11}^3)\, q_{30}q_{40}^2 + [630q_{11}^2 q_{30}^2 q_{31} + (1050q_{11}q_{21}^2 + 2184q_{11}^2 q_{21} + 600q_{11}^3)\, q_{30}^2]\, q_{40} + (525q_{11}q_{22} - 525q_{12}q_{21})\, q_{30}^4 - (350q_{21}^3 + 2100q_{11}q_{21}^2 + 1176q_{11}^2 q_{21} + 1072q_{11}^3)\, q_{30}^3\}/(18{,}900q_{11}^3 q_{30}^3)$$

$$y_5 = 2y_2^4 - 3y_2 y_4$$

[a] $q_{ij} = (\partial^{i+j} p/\partial\rho^i\, \partial T^j)$ evaluated at ρ_c and T_c.

coefficients of the Padé have been chosen such that at $T=0$, $x=0$ and $y=3$. The series representation provides a good approximation down to temperatures of about $0.7T_c$. The [7/8] Padé appears to work well for all temperatures below T_c. (Note: the [7/8] Padé has been forced to give the correct result at $T=0$.)

2.4. Near $T=0$

Although classical model fluids are not generally used to represent fluid properties at very low temperatures, calculations of the phase diagram of a given model often include the low-temperature behavior for the sake of completeness. The three canonical methods for solving the equilibrium conditions, as well as the f–g method we have described, are not very useful near $T=0$ because the coexistence curve has essential singularities at $T=0$. These singularities make numerical computations very difficult. In the case of the van der Waals model the [7/8] Padé approximant to the series representation of $T(x)$ works well, but on all other models that we have investigated, we have not found a Padé that, when forced to give the correct $T=0$ values for x and y, does not have extraneous zeros or poles at higher temperatures.[22]

We suggest that if the low-temperature portion of the coexistence curve must be calculated, then f and g be used to obtain asymptotic expansions about $T=0$. For the van der Waals model we find, to "lowest order,"

$$y=3-8T/9 \tag{25}$$

and

$$x=\frac{81}{8T}\exp\left(-\frac{27}{8T}\right) \tag{26}$$

A more complete representation is provided by

$$\begin{aligned} x=\lambda+\lambda^2(2/z+2/3+4z/9+4z^2/27+\cdots) \\ +\lambda^3[6/z^2+10/(3z)+49/18+40z/27+20z^2/27+\cdots] \\ +\cdots \end{aligned} \tag{27}$$

$$T=9z/8-3z^2/8+\lambda z^2/8+\lambda^2(z/8+z^2/12+\cdots)+\cdots \tag{28}$$

where $\lambda=3(3-z)\exp[-(3+z)/z]$ and $z=3-y$.

3. MULTICOMPONENT AND POLYDISPERSE FLUIDS

When the fluid consists of a mixture (discrete and/or polydisperse) the dew/bubble conditions are more difficult to solve because one must also determine the composition of the dew or bubble phase, i.e., the solution involves additional variables. In these cases the geometry associated with the dew/bubble conditions is no longer two-dimensional and thus is more difficult to visualize. This has tended to lead to solution algorithms that we would tend to classify as "blind-search" methods. That is, the methods tend to use numerical searching algorithms that do not rely very much on the geometry associated with the dew/bubble conditions. The utility of these algorithms begins to decrease rapidly as the number of components in the mixture increases. (In practical applications utility is synonymous with computational speed.) When the fluid is polydisperse, there is in effect an infinite number of components, and the blind-search methods are not very useful.

In this section we shall discuss new methods that have been devised to solve the dew/bubble conditions for mixtures with very many components. We begin by briefly describing two methods that grew out of recent investigations of phase equilibrium in polydisperse fluids (Sections 3.1 and 3.2), followed by a more detailed description of our recent work on this problem (Section 3.3). Our recent work does not yet enjoy as wide a range of applicability as the other two methods, but it is a method more directly tied to the geometry associated with the dew/bubble conditions, and we believe, therefore, that it represents an important step toward a more general and quite powerful method.

3.1. Perturbation Expansions

Gualtieri *et al.*,[4] Johnson *et al.*,[5] Briano and Glandt,[7] Kincaid *et al.*,[6] and Kofke and Glandt[10] have developed methods that determine the properties of a polydisperse fluid, in particular the phase boundaries, that are based upon the properties of some reference system, the properties of which are assumed to be known completely. In these methods the dew/bubble curve is that of the reference system plus corrections that depend on the differences between the reference system and the system of interest. These methods can be quite effective, but only in certain regions of the phase diagram. In particular, the perturbation expansions do not work (i.e., converge) in those regions of the phase diagram where the phase boundaries of the reference system are not qualitatively the same as those of the system of interest. For example, if the reference system is a pure fluid and the condentherm temperature T_0 is greater than the critical

temperature of the reference system, there is no way for the perturbation methods to generate the dew/bubble curves or temperatures in the interval $(T_{c,\,1\text{-comp}},\ T_0)$.

3.2. Quadrature Methods

The quadrature method is an ingenious and effective method, first described by Cotterman and Prausnitz[14] [see also refs. 15 and 16], for correcting the deficiencies of pseudocomponent schemes. The essential feature of the method is to choose C' pseudocomponents in a way that provides an accurate description of the composition of the mixture *as well as* an accurate approximation to some functions of $\{f_i\}$. (Here C' is usually much smaller than C.) More precisely, $\sum_{i=1}^{C} f_i = 1$ is approximated by the integral $\int F(I)\,dI$, where $F(I)$ is the mole-fraction distribution density. Then $\int F(I)\,dI$ is replaced by $\sum_{k=1}^{C'} w(I_i)\,F(I_k)$, where $w(I_k)$ and I_k are the weight factors and nodes, respectively, of the Gaussian quadrature approximation to $\int F(I)\,dI$. Cotterman and Prausnitz showed that their quadrature method provided more accurate descriptions of phase equilibrium than several commonly used pseudocomponent methods when C' is the same for each method. This is a splendid result, because it provides greater accuracy without having to introduce a completely new solution algorithm for solving the equilibrium conditions.

Although this method provides a way that in some sense reduces the number of components, ultimately some type of numerical searching scheme must be implemented in order to solve the equilibrium conditions. It is precisely this numerical searching scheme that is the focus of our investigation. This method can suffer from the same geometric defect that the perturbation method has: the coexistence surface of a C'-component mixture can not always closely approximate the coexistence surface of a C-component mixture when $C' < C$.

3.3. Two New Approaches

The two methods that we describe below are not limited by the defects that the perturbation and quadrature methods possess. Although they cannot be used on as broad a class of models at present, we think there is a reasonable probability that they can eventually be generalized. We begin our discussion of these two methods with a description of the dew/bubble conditions and then develop the methods along lines similar to those described in Section 2 for one-component systems.

The dew/bubble conditions for a polydisperse fluid are

$$p(T, x \mid F) = p(T, y \mid F_y) \tag{29}$$

$$\mu(I, T, x \mid F) = \mu(I, T, y \mid F_y) \tag{30}$$

$$\int F_y \, dI = 1 \tag{31}$$

The chemical potential depends only explicitly on F through the ideal mixing term $k_B T \ln F(I)$; all other dependence on F will be through a set of functionals $\{w_i\}$ of F. Thus, we define $\hat{\mu}$ by

$$\mu(I, T, \rho, \{w_j\}) = k_B T \ln F(I) + \hat{\mu}(I, T, \rho, \{w_j\}) \tag{32}$$

Equation (30) may be rearranged to yield

$$F_y(I) = F(I) \exp \frac{\hat{\mu}_x - \hat{\mu}_y}{k_B T} \tag{33}$$

Substituting this expression into Eq. (31), we obtain

$$\int F(I) \exp \frac{\hat{\mu}_x - \hat{\mu}_y}{k_B T} \, dI = 1 \tag{34}$$

The dew/bubble equations may now be transformed into

$$f(T, x, y \mid F, F_y) = p(T, x \mid F) - p(T, y \mid F_y) = 0 \tag{35}$$

and

$$g(T, x, y \mid F, F_y) = \int F(I) \exp \frac{\hat{\mu}_x - \hat{\mu}_y}{k_B T} \, dI - 1 = 0 \tag{36}$$

with

$$F_y(I) = F(I) \exp \frac{\hat{\mu}_x - \hat{\mu}_y}{k_B T} \tag{37}$$

These equations look similar to the one-component dew/bubble conditions, but they are still quite different because F_y is not explicitly determined. There is still life in the f and g curves, however, if the functionals $\{w_i\}$ can somehow be eliminated. How to do this in general is not yet clear. But it can be done for a large class of models;[8] it is easy to do for

the simple model fluids given in Table II. For these models, f and g depend on F_y only through

$$z_y = \int IF_y(I)\, dI \tag{38}$$

That is, for the models listed in Table II, explicit expressions for z_y can be obtained as functions of T, x, and y. Such expressions are obtained by substituting Eq. (37) into Eq. (38) and solving for z_y in terms of T, x, and y. For these models the dew/bubble conditions become

$$f(T, x, y) = 0 \tag{39}$$

$$g(T, x, y) = 0 \tag{40}$$

just as in the one-component case. Once Eqs. (39) and (40) are solved for $x(T)$ and $y(T)$, $F_y(I)$ is immediately obtained from Eq. (37).

Table II. Functions Defining Models 1, 2, and 3

Model 1 [van der Waals, $b(I) = b_0 + b_1 I$, $a(I, J) = 1$]

$$p(T, \rho, z) = \frac{8T\rho}{3 - \rho(b_0 + b_1 z)} - 3\rho^2$$

$$\mu(I, T, \rho \mid F) = T\left[\ln F(I) + \ln\left(\frac{\rho}{3 - \rho(b_0 + b_1 z)}\right) + \left(\frac{\rho(b_0 + b_1 I)}{3 - \rho(b_0 + b_1 z)}\right)\right] - \frac{9}{4}\rho$$

$$z_y = \frac{1}{1 - 3(x^2 - y^2)b_1/(8Tv)}$$

Model 2 [van der Waals, $b(I) = 1$, $a(I, J) = (I + J)/2$]

$$p(T, \rho, z) = \frac{8T\rho}{3 - \rho} - 3\rho^2 z$$

$$\mu(I, T, \rho \mid F) = T\left[\ln F(I) + \ln\left(\frac{\rho}{3 - \rho}\right) + \frac{\rho}{3 - \rho}\right] - \frac{9}{8}\rho(z + I)$$

$$z_y = \frac{1}{1 + 9(x - y)/(8Tv)}$$

Model 3 [Soave–Redlich–Kwong, $b(I) = 1$, $a(I, J) = (I + J)/2$]

$$p(T, \rho, z) = \frac{8T\rho}{3 - \rho} - \frac{9\rho^2 z}{3 + \rho}$$

$$\mu(I, T, \rho \mid F) = T\left[\ln F(I) + \ln\left(\frac{\rho}{3 - \rho}\right) + \frac{\rho}{3 - \rho}\right] - \frac{27}{8}\left[\frac{\rho z}{3 + \rho} + \ln\left(1 + \frac{\rho}{3}\right) \times I\right]$$

$$z_y = \frac{v}{v - (27/8T)\ln[(3 + y)/(3 + x)]}$$

3.3.1. The Geometry of the *f* and *g* Curves. The f and g curves of the mixture bear a close resemblance to those of the one-component fluid. There are, however, some important distinctions:

1. The curves are no longer symmetric about the line of trivial solutions $x = y$.
2. The curves are tangent as they cross the line $x = y$, but these points no longer can be identified with spinodal points.
3. As the critical point is approached, the curves do not shrink to a point; rather, a nontrivial crossing point of the curves moves to the $x = y$ line.
4. Above T_c the curves maintain nontrivial crossing points, until at the condentherm temperature T_0 they become tangent at a single point; for $T > T_0$ the curves do not intersect.

Figure 10 illustrates these features for model 2.

It is still useful in the case of mixtures to introduce $\tilde{f}$ and $\tilde{g}$ defined by Eqs. (35) and (36), especially for numerical computations, but $\tilde{f}$ will not

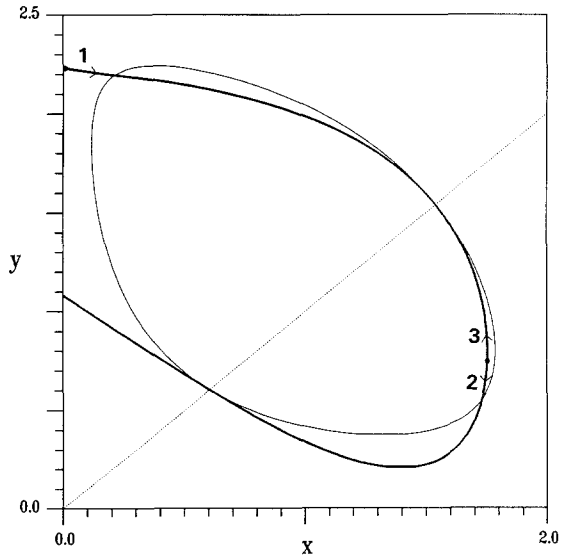

Fig. 10. The f and g curves (thick and thin curves, respectively) for model 2 in the density–density plane for $T = 0.9$ ($v = 10$). The dotted line represents the trivial solutions, $x = y$. The nontrivial intersections of the f and g curves represent solutions of the dew/bubble conditions, x is the density of the bulk phase, and y is the density of the dew/bubble. The search for the nontrivial solutions follows paths 1 and 2. If no solution is found along path 2, path 3 is taken (this is required only at temperatures near and above T_c).

necessarily be polynomial in x and y (see model 3). Also, the $\tilde{f}$ and $\tilde{g}$ curves are not always closed loops, as shown in Fig. 11. The additional thermodynamic degrees of freedom in mixtures may allow additional fluid phase transitions. These transitions manifest themselves through the appearance of additional branches of the f curve and the absence of a closed loop for the g curve. If the f curve is polynomial, the appearance of additional phase transitions is easy to detect by determining the number of real roots of $\tilde{f}=0$ for fixed T and x.

Model 1 provides a good illustration of this latter point. For fixed T and x, $\tilde{f}=0$ is a quartic polynomial in y. For a range of T there are four real roots instead of two. (See Fig. 11.)

3.3.2. Numerical Solutions. Our numerical solution method for the dew/bubble conditions is indicated schematically in Fig. 10. It is basically similar to the one used for the one-component case, except that, since the f and g curves are not symmetric about the line $x=y$, it must also locate an additional crossing of the two curves. The basic strategy is the same: follow the f curve until it crosses the g curve. The dew/bubble curves shown in Figs. 6 and 12 were obtained using this method. The dew/bubble

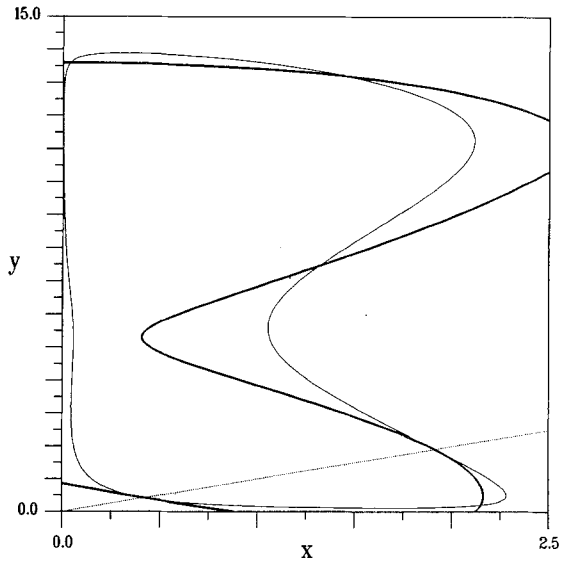

Fig. 11. The f and g curves (thick and thin curves, respectively) for model 1 in the density–density plane for $T=0.7$ ($v=10$, $b_0=0.12$, $b_1=0.88$). For this model additional equilibrium states are possible, as indicated by the multiple crossing points of the f and g curves. In this particular case the two crossing points for which x is approximately 1.5 are not mechanically stable.

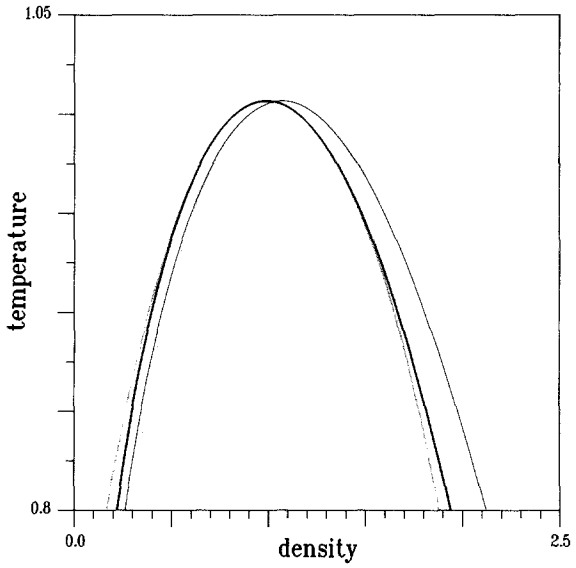

Fig. 12. The dew/bubble (thick curve) and shadow (thin curve) curves for model 1 in the temperature–density plane for $v = 10$ and $b_0 = 1/2$. The dotted curves represent the 5-term series-expansion result.

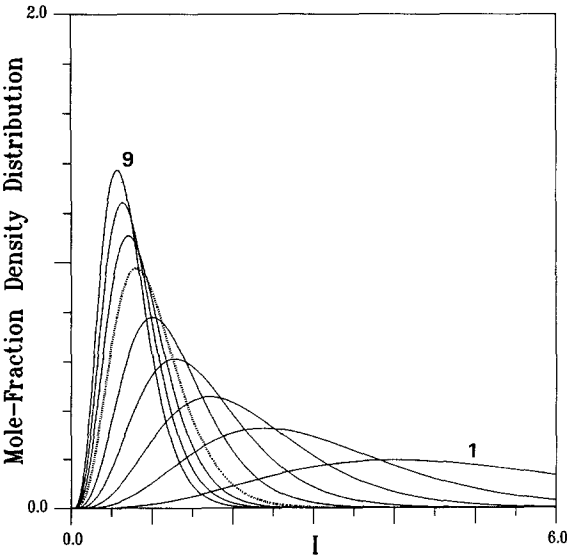

Fig. 13. The mole-fraction density distribution F_y as a function of species label for model 2 ($v = 5$, see Fig. 6). The nine curves represent F_y at nine different points on the shadow curve. Curve 1 is for the point $y = 2.85$, $T = 0.8$; curve 9 is for the point $y = 0.529$, $T = 0.8$. The sixth curve (dotted) is drawn at the critical density and temperature. At that point $F(I) = F_y(I)$. Thus, the dotted curve also indicates $F(I)$.

curves do not, of course, show the composition of the shadow phase. However, given the dew/bubble curves, it is a simple matter to determine $F_y(I)$ using Eq. (37). In Fig. 13 we plot $F_y(I)$ for several temperatures.

Near the condentherm points (X_0, T_0) and (Y_0, T_0) (see Fig. 6) the crossing points of the f and g curves are quite close to each other, and between the crossing points the two curves are nearly identical. In this region it is difficult to maintain enough numerical precision to locate accurately the dew/bubble curve. We find it necessary to determine T_0, X_0, and Y_0 using another method. In the neighborhood of the condentherm points we represent the dew/bubble and shadow curves by

$$y = Y_0 + \sum_{i=1} Y_i (x - X_0)^i \tag{41}$$

$$T = T_0 + \sum_{i=1} T_i (x - X_0)^i \tag{42}$$

Substituting these expansions into Eqs. (39) and (40), we find that T_0, X_0, and Y_0 are determined by

$$f(T_0, X_0, Y_0) = 0 \tag{43}$$

$$g(T_0, X_0, Y_0) = 0 \tag{44}$$

and

$$f_x(T_0, X_0, Y_0)\, g_y(T_0, X_0, Y_0) - f_y(T_0, X_0, Y_0)\, g_x(T_0, X_0, Y_0) = 0 \tag{45}$$

where the subscripts on f and g indicate partial derivatives. We solved these equations with a "blind-search" algorithm using initial guesses for T_0, X_0, and Y_0 obtained from the calculated dew/bubble curves. We note that although this "brute force" method was more reliable than our dew/bubble algorithm, it is still quite difficult to maintain adequate numerical precision during the calculations. In Figs. 14 and 15 we show how T_0, X_0, and Y_0 depend on $1/\nu = \mathrm{var}(F(I))$. [We choose $F(I) = \nu^\nu I^{\nu-1} \exp(-\nu I)/\Gamma(\nu)$.]

The point at which the dew bubble and shadow curves cross is the critical point, denoted by the point C in Fig. 6. Our values for T_c and X_c shown in Figs. 14 and 15 were obtained by simple linear interpolation of the dew/bubble curve data.

3.3.3. Solution by Series Expansions. The numerical procedures described above are useful because, with proper attention to the numerical precision problems that arise, they guarantee a numerically exact representation of the dew/bubble curves. The numerical procedures are also based on a simple geometrical representation of the dew/bubble conditions,

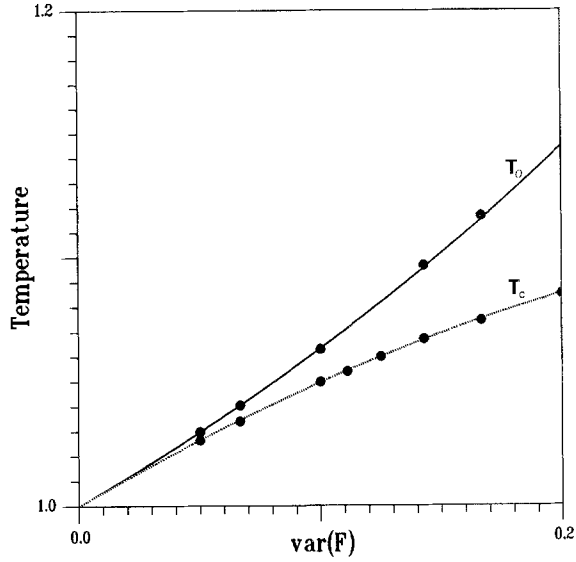

Fig. 14. The condentherm temperature T_0 and critical temperature T_c for model 2 as a function of the variance of $F(I)$, which in this case is $1/v$. The dots are values located numerically; the curves represent the series-expansion results.

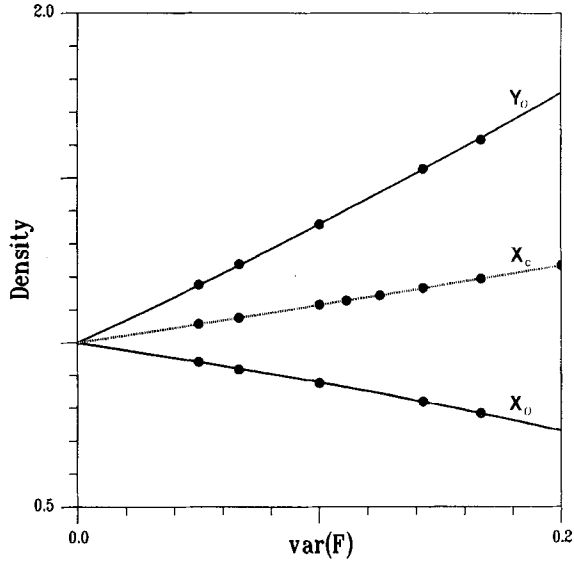

Fig. 15. The condentherm densities X_0 and Y_0 and the critical density X_c for model 2 as a function of the variance of $F(I)$ [$\text{var}(F) = 1/v$ in this case]. The dots are values located numerically; the curves represent the series-expansion results.

so that when computational difficulties arise, or when the phase behavior becomes more complicated, one can always use the graphs of the f and g curves to suggest modifications of the algorithm. However, like all other numerical schemes for solving equilibrium conditions, the method is rather tedious. An alternative to numerical algorithms is the method of series expansion. The results described below indicate that series expansion may prove to be a very useful (i.e., efficient) method for solving the dew/bubble conditions. Even more intriguing is the very likely possibility that the series expansion method can be used on a much broader class of models than we consider here.

The method is conceptually quite simple: given T_0, X_0, and Y_0 [and, of course, $f(T, x, y)$ and $g(T, x, y)$], represent the dew/bubble curves by the expansions given in Eqs. (41) and (42); the coefficients Y_i and T_i are determined by expanding the equations

$$f(T(x), x, y(x)) = 0 \tag{46}$$

and

$$g(T(x), x, y(x)) = 0 \tag{47}$$

about the point $x = X_0$. This method will be useful if enough coefficients Y_i and T_i can be determined so that Eqs. (41) and (42) yield an accurate representation of the dew/bubble curves.

One can also determine T_0, X_0, Y_0, T_c, and X_c using a series expansion method. For these models the dew/bubble curves collapse onto the one-component coexistence curve in the limit $1/\nu = \text{var}(F) \to 0$. In that limit T_0 and $T_c \to T_{c,\text{1-comp}} = 1$ and X_0, Y_0, and $X_c \to X_{c,\text{1-comp}} = 1$. Thus, setting $\varepsilon = 1/\nu$,

$$X_0 = 1 + \sum_{i=1} A_i \varepsilon^i \tag{48}$$

$$Y_0 = 1 + \sum_{i=1} B_i \varepsilon^i \tag{49}$$

and

$$T_0 = 1 + \sum_{i=1} C_i \varepsilon^i \tag{50}$$

one can obtain the coefficients A_i, B_i, and C_i by substituting Eqs. (48)–(50) into Eqs. (43)–(45) and expanding about $\varepsilon = 0$. The series-expansion results are compared to the numerically exact results in Figs. 14 and 15. It seems clear to us that this approach is quite promising. A complete description of this technique is given in refs. 21 and 9.

4. CONCLUSIONS

Even though the phase space of a complex mixture is quite large, we hope that the examples we have discussed above make it clear that comprehensible descriptions of the phase behavior of such systems is possible. We think that the series-expansion method will prove to be an extremely effective technique. The Padé approximants of the series provide closed (approximate) expressions for the dew/bubble curves. The series coefficients can be determined symbolically and can include parameters so that entire classes of models may be dealt with easily.[9,21] For applications where more accurate solutions are desired, the Padé representation can be used as a first guess for other algorithms, and thereby ensure a greater likelihood of convergence. Furthermore, it seems likely that similar methods can be developed to solve the full equilibrium conditions.

Our series-expansion method for the dew/bubble curve works well because the expansion is made around the extremal points of the dew/bubble curves—not about the critical point. To obtain a series representation of the entire coexistence surface, we expect that the expansion will have to be centered along the "top" of the coexistence surface.

ACKNOWLEDGMENTS

We pay tribute in this Festschrift to the outstanding scientific and professional contributions that Prof. E. G. D. Cohen has made during his first 65 years. We would, in addition, like to express our appreciation of his great talent as a teacher and counselor. We can find no better rule by which to measure professional and personal achievements than by the standards that he has set and continues to set.

This work was supported by the Office of Basic Energy Sciences, U.S. Department of Energy, under contract DE-FG02-87ER13648.

REFERENCES

1. J. M. J. van Leeuwen and E. G. D. Cohen, *Phys. Rev.* **176**:385 (1968).
2. P. Domanski and D. Didion, Computer modeling of the vapor compression cycle with constant flow area expansion device, Nat. Bur. Stand. (U.S.) Bldg. Sci. Ser. 155 (May 1983).
3. H. B. Callen, *Thermodynamics and Introduction to Thermostatistics*, 2nd ed. (Wiley, New York, 1985).
4. J. A. Gualtieri, J. M. Kincaid, and G. Morrison, *J. Chem. Phys.* **77**:521 (1982).
5. K. A. Johnson, D. A. Jonah, J. M. Kincaid, and G. Morrison, *J. Chem. Phys.* **82**:5178 (1985).
6. J. M. Kincaid, R. A. MacDonald, and G. Morrison, *J. Chem. Phys.* **87**:5425 (1987).
7. J. G. Briano and E. D. Glandt, *Fluid Phase Equil.* **14**:91 (1983).

8. J. M. Kincaid, M. Azadi, G. Fescos, L. Pellizzi, and K. B. Shon, Phase equilibrium in a special class of polydisperse fluid models, *J. Chem. Phys.*, in press (1989).
9. G. Fescos, J. M. Kincaid, and G. Morrison, New methods for locating phase boundaries, *Int. J. Thermophys.*, in press (1989).
10. D. A. Kofke and E. D. Glandt, *J. Chem. Phys.* **90**:439 (1989).
11. R. L. Cotterman, R. Bender, and J. M. Prausnitz, *Ind. Eng. Process Des. Dev.* **24**:194 (1985).
12. E. Hendricks, Reduction theorem for phase equilibrium problems, *Ind. Eng. Chem. Proc.* (1988); Perturbation method for phase equilibrium calculations, preprint (1988).
13. A. G. Schlijper, *Fluid Phase Equil.* **34**:149 (1987).
14. R. L. Cotterman and J. M. Prausnitz, *Ind. Eng. Process Des. Dev.* **24**:434 (1985).
15. R. A. Behrens and S. I. Sandler, SPE/DOE report #14925 (1986); S. K. Shibata, S. I. Sandler, and R. A. Behrens, *Chem. Eng. Sci.* **42**:1977 (1987).
16. G. F. Chou and J. M. Prausnitz, *Fluid Phase Equil.* **30**:75 (1986).
17. L. D. Landau, *Zh. Eksp. Teor. Fiz.* **7**:19, 637 (1937) [*Collected Papers of L. D. Landau*, D. ter Haar, ed. (Pergamon, Oxford, 1965), No. 29].
18. H. E. Stanley, *Introduction to Phase Transitions and Critical Phenomena* (Oxford University Press, New York, 1971).
19. J. M. Kincaid and E. G. D. Cohen, *Phys. Rep.* **22C**:57 (1975).
20. G. Morrison and M. O. McLinden, Application of a hard sphere equation of state to refrigerants and refrigerant mixtures, Nat. Bur. Stds. (U.S.) Technical Note 1226 (August 1986).
21. G. Fescos, Series solutions to the dew/bubble conditions for two polydisperse fluid models, M. S. Thesis, Department of Mechanical Engineering, SUNY at Stony Brook (1988).
22. J. M. Kincaid, B. Tucker, and G. Stell, Representation of pure fluid coexistence curves by series expansion, SUSB CEAS Report No. 542 (February 1989).